

Thermal and structural characteristics of the AM50 magnesium alloy

W. Kasprzak ^{a, c, *}, J.H. Sokolowski ^b, M. Sahoo ^a, L.A. Dobrzański ^c

^a CANMET Materials Technology Laboratory, 568 Booth Street, Ottawa, Ontario, K1A 0G1, Canada

^b Light Metals Casting Technology Group, University of Windsor, 401 Sunset Avenue, Windsor, Ontario, Canada, N9B 3P4

^c Division of Materials Processing Technology, Management and Computer Techniques in Materials Science, Institute of Engineering Materials and Biomaterials, Silesian University of Technology, ul. Konarskiego 18a, 44-100 Gliwice, Poland

* Corresponding author: E-mail address: wojciech.kasprzak@nrcan.gc.ca

Received 26.03.2008; published in revised form 01.06.2008

Materials

ABSTRACT

Purpose: The goal of this publication is to demonstrate the laboratory metal casting simulation methodology based on controlled melting and solidification experiments. The thermal characteristics of the AM50 magnesium alloy during melting and solidification cycles were determined and correlated with the test samples' microstructural parameters.

Design/methodology/approach: A novel methodology allowed to perform variable solidification rates for stationary test samples. The experiments were performed using computer controlled induction heating and cooling sources using Argon for melt protection and test sample cooling.

Findings: Thermal analysis data indicated that the alloy's melting range was between approximately 434 and 640°C. Increasing the cooling rate from 1 to 4°C/s during solidification process reduced the Secondary Dendrite Arm Spacing from approximately 64 to 43µm. The temperatures of the metallurgical reactions were shifted toward the higher values for faster solidification rates. Fraction liquid curve indicates that at the end of melting of the $\alpha(\text{Mg})$ - $\beta(\text{Mg}_{17}\text{Al}_{12})$ eutectic, i.e., 454.2°C the alloy had a 2% liquid phase.

Research limitations/implications: Future research is intended to address the development of a physical simulation methodology representing very high solidification rates used by High Pressure Die Casting (HPDC) and to assess the microstructure refinement as a function of solidification rates.

Practical implications: Advanced simulation capabilities including non-equilibrium thermal and structural characteristics of the magnesium alloys are required for the development of advanced metal casting technologies like vacuum assisted HPDC and its heat treatment.

Originality/value: The presented results point out the direction for future research needed to simulate the alloy solidification in a laboratory environment representing industrial casting processes.

Keywords: Casting; AM50 alloy; Thermal analysis; Solidification

1. Introduction

Interest in magnesium alloy technologies for automotive applications has grown over the last 60 years since its first

application for the VW beetle in 1946. Recent requirements for reduction of vehicle weight has triggered a stronger interest in magnesium applications due to tighter emission requirements. Unfortunately, unstable magnesium prices and a lack of large scale applications in the past resulted in limited research and

development activities [1]. As of 2005 the magnesium components in a passenger vehicle amounted to approximately 6 kg, i.e., 0.3% of its overall weight. It is forecasted that by 2015 this weight is expected to increase to approximately 11kg and in 2020 to approximately 100 kg per vehicle. To date magnesium alloys were successfully used for selected automotive structural and powertrain applications like engine cradles, seat frames, instrument panels, transmission housings, etc [26-29]. The magnesium recycling activities have to be properly addressed together with the development of new high temperature alloys to fulfill sustainable growth requirements.

Low melting point of magnesium alloys sets a natural limit to their service temperature. Improvement of magnesium high temperature properties might lead to its wider application for selected powertrain applications if current temperature limit, i.e. $\sim 150^{\circ}\text{C}$ can be exceeded. Hybrid structures combining cast-in Mg and Al based components might be an intermediate solution to overcome magnesium limitations for elevated temperature applications. A recent example could be the Mg/Al sandwich engine block introduced into commercial passenger vehicles by BMW.

Development of advanced magnesium manufacturing techniques and processing technologies, like vacuum HPDC, thixomolding and magnesium sheet rolling require advanced knowledge of the alloy's behaviour under non-equilibrium solidification conditions. A scientifically sound understanding of alloy's solidification process and its corresponding structural characteristics is crucial [2-5]. The design of an energy efficient heat treatment processes requires a detailed knowledge of the effect of the solidification rate on the cast microstructure since its refinement and corresponding segregation will have an impact on the dissolution kinetics of the intermetallic phases during the solution treatment [6-8]. Advanced laboratory simulation capabilities including controlled melting, solidification and quenching combined with thermal analysis are required to properly address this issue. An understanding of the complex metallurgical relations including the effect of the solidification rates on alloy fraction solid evolution, liquidus temperature, etc. are necessary for the development of an adequate data base for computational modeling [3, 9, 10].

The common laboratory casting practice is to use a variety of molds with different thermal conductivities having various geometries to achieve the desired solidification rate and corresponding microstructural refinement. Flexibility to control the cooling rate is rather limited and the qualities of any in-situ temperature measurements are not satisfactory due to the high thermal mass of the mold and multi-directional heat extraction conditions. It is a common practice to assume that the laboratory test bar represents the specific section of the industrial cast component as well as indicates an overall melt quality. The microstructure refinement level is the only reliable parameter allowing for the link between industrial component and the laboratory casting experiments.

In the present study a novel laboratory methodology was used to simulate the melting and solidification processes for a common magnesium casting alloy AM50. This approach achieves various microstructural refinement levels for macro size test samples as well as determines solidification rates and the corresponding thermal characteristics of the alloy. Laboratory solidification experiments could be tailored to match selected casting sections. Representative macro test samples could be used for simulation of the casting post processing operations such as heat treatment followed by comprehensive metallurgical and mechanical properties evaluations.

2. Experimental procedures

The material used for this study was an AM50 alloy with the chemical composition listed in Table 1. This alloy has a good combination of castability and ductility and is frequently used for low and high pressure die cast components [11-17]. An additional T6 heat treatment could be used to increase the strength of the as-cast components [17]. A cylindrical test samples with a diameter of $\phi = 16\text{mm}$ and a length of $l = 18\text{mm}$ were taken from the ingot. Each sample had a predrilled hole to accommodate a thermocouple positioned at the center of the test sample to collect the thermal data and control the processing temperatures. The size of the macro test sample was sufficient for subsequent metallurgical analysis including metallography and selected mechanical testing.

Table 1.
Chemical composition of the AM50 alloy, wt%

Al	Mn	Si	Zn	Fe
5.25	0.37	0.02	0.01	0.004

The thermal analysis during melting and solidification cycles was carried out using the Universal Metallurgical Simulator and Analyzer (UMSA) [18]. The test samples were processed in low thermal mass steel foil and the top and bottom were insulated using low density ceramic ($\sim 0.28\text{ g/cm}^3$). This design considerably reduced the thermal inertia, improved the thermal signal and reduced the noise. In order to assure a rapid temperature response, very low thermal mass K type thermocouples were utilized. The melting and solidification experiments for the AM50 alloy were carried out using cover gases. A conventional CO_2/SF_6 gas mixture was evaluated within the scope of this work but Argon was also used for experiments due to its reasonable melt protection capabilities and low hazard risk particularly in the laboratory environment.

The procedure comprised of the following steps. First, the test sample was heated to $700 \pm 0.2^{\circ}\text{C}$ and isothermally kept at this temperature for a period of 5 minutes in order to stabilize the melt conditions. Next, the test sample was solidified at cooling rate of approximately 1°C/s , that was equivalent to the solidification process under natural cooling conditions, and a 4°C/s average solidification rate. The Argon gas at 8 bars pressure and at a flow rate of up to 50 LMP (Liters Per Minute) was used to cool the outer surface of the test sample to accelerate the solidification process. A variable solidification rate allowed for flexible control of the as-cast microstructure representative of selected commercially available cast components.

The thermal analysis signal in the form of heating and cooling curves was recorded during the melting and solidification cycles. The temperature vs. time and the first derivative vs. temperature curves as well as the fraction liquid/fraction solid vs. temperature curves were calculated and plotted. The melting rate was calculated between the solidus (start of the melting process) and the liquidus (end of the melting process) temperatures, i.e., 433.7 and 640.1°C and was equal to approximately 0.8°C/s . The average solidification rate was calculated between the non-equilibrium liquidus and the solidus temperatures [4-6]. The novel fraction liquid curve was determined during the melting cycle by calculating the cumulative surface area between the first

derivative of the heating curve and the base line. The base line represented the hypothetical first derivative of the melting curve that did not exhibit phase transformation during the melting process [19]. The area between the two derivative curves (calculated between the solidus and liquidus temperatures) was proportional to the heat of melting. Therefore, the melting heat directly delivered to the test sample affected the fraction liquid evolution. Similar calculations were performed for the fraction solid except that fraction solid was proportional to the latent heat released during the solidification process [19].

After completion of the experiments the longitudinal metallographic sections were prepared and light optical microscopy observations together with image analysis were performed to assess the microstructural changes caused by various solidification conditions. Test samples were etched with acetic glycol for 15 seconds to reveal their microstructures. The Secondary Dendrite Arm Spacing (SDAS) was measured using intercept method. Thirty (30) analytical fields were analyzed and the average values of the SDAS with corresponding standard deviation were calculated. The representative optical micrographs under 50 and 500x magnifications were taken.

The so called controlled ignition test was carried out in ambient atmosphere to evaluate alloy behaviour during liquid metal processing. This simulation methodology can be used to determine operating procedures for magnesium melting and solidification experiments. Moreover, experimental results can be used for optimization of heat treatment parameters and cover gas selection with respect to alloy oxidization during its thermal processing [29].

3. Results

3.1. Thermal analysis during controlled melting and solidification

The AM50 alloy microstructure consisted of an $\alpha(\text{Mg})$ matrix, a $\alpha(\text{Mg})$ - $\beta(\text{Mg}_{17}\text{Al}_{12})$ eutectic as well as an Al_8Mn_5 phase [7, 8, 11, 12]. Under equilibrium solidification conditions the AM50 alloy should not contain the eutectic phase constituents because the Al concentration is below the solid solubility limit of Al in Mg at the eutectic temperature [11, 13]. Most likely this indicates that the $\alpha(\text{Mg})$ - $\beta(\text{Mg}_{17}\text{Al}_{12})$ eutectic is a non-equilibrium eutectic formed during the accelerated solidification. Detailed semi-equilibrium solidification experiments using the DSC (Differential Scanning Calorimeter) apparatus revealed similar observations [20, 21]. Since commercial castings very seldom solidify under semi-equilibrium conditions the non-equilibrium microstructure is expected to be dominant.

Thermal analysis revealed that the melting process of the AM50 alloy started at $433.7 \pm 1^\circ\text{C}$ and was completed at $640.1 \pm 1.5^\circ\text{C}$. Above this temperature the alloy was in a liquid state. Exceeding this temperature increased the alloy's superheat (Figure 1 and Table 2a). The thermal analysis heating curve could be used to determine the optimum process parameters for the solution treatment operation. Exceeding 433.7°C during the single step solution treatment (using rapid heating) would result in incipient melting of the non-equilibrium $\alpha(\text{Mg})$ - $\beta(\text{Mg}_{17}\text{Al}_{12})$

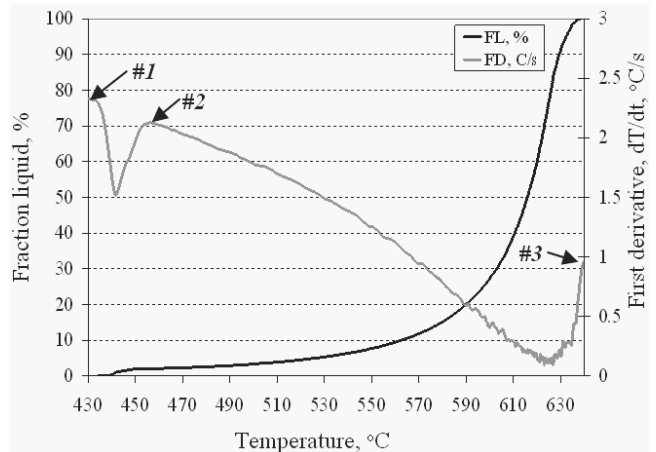


Fig. 1. Temperature vs. fraction liquid (FL) and first derivative (FD) curves recorded during the melting of the AM50 alloy test sample at a 0.8°C/s heating rate. The numbers correspond to the various metallurgical reactions as presented in Table 2a

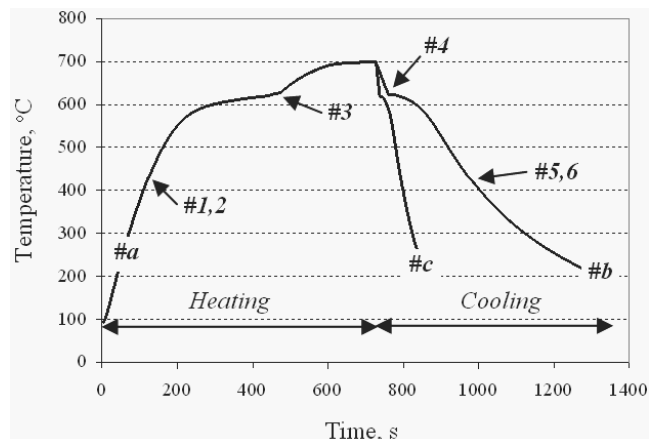


Fig. 2. Temperature vs. time curves of the AM50 alloy test samples recorded during melting at a 0.8°C/s (#a) and solidification at 1°C/s (#b) and 4°C/s (#c). The numbers correspond to the various metallurgical reactions as presented in Tables 2a, b

eutectic phase. The as-cast microstructure refinement level as well as the heating rate to solution treatment temperature should be considered during the heat treatment optimization experiments since these factors have an effect on the dissolution kinetics of the intermetallic phases during the solution treatment operation.

Analysis of the fraction liquid and first derivative curve (Figure 1) provides a good understanding of the phase transformation during the heating cycle as well as the corresponding volume of the liquid phase that evolved during the melting process. Figure 1 indicates that at the end of dissolution of the $\alpha(\text{Mg})$ - $\beta(\text{Mg}_{17}\text{Al}_{12})$ eutectic, i.e., 454.2°C , the alloy had a 2% liquid phase located between the magnesium dendrites. Increasing the temperature during the alloy melting process

resulted in a gradual increase in the liquid phase that reached 100% volume at approximately 640.1°C (Figure 1 and Table 2a). This data has practical implications for selecting the magnesium ingot preheating temperature for semi-solid processing. For this type of operation an exact ratio between the volume of liquid / solid phase is required. Conventionally, the volume of the liquid phase is estimated using quenching experiments combined with metallographic evaluations. This method is time consuming and can render considerable experimental and analytical errors and also make it unsuitable for on-line applications.

Temperature vs. time cooling curves recorded for the test samples heated to 700°C and solidified at 1°C/s are presented in Figure 2. Two visible temperature arrests were noted on the cooling curves. More detailed information pertaining to the alloy's thermal characteristics such as non-equilibrium liquidus, nucleation of the $\alpha(\text{Mg})$ - $\beta(\text{Mg}_{17}\text{Al}_{12})$ eutectic, etc. were determined using the first derivative curves. The representative first derivative vs. temperature curves are presented in Figure 3 (#b). The temperatures of the metallurgical reactions are pointed out by numbers and the corresponding numerical values are presented in Table 2b. Based on the cooling curve analysis the non-equilibrium liquidus temperature was found to be at 625.1°C (Figure 3). At this temperature the first magnesium dendrites,

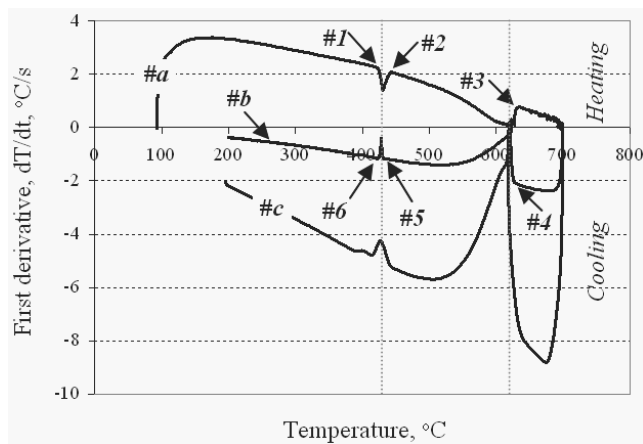


Fig. 3. First derivative (heating / cooling rate) vs. temperature curves of the AM50 alloy test samples recorded during melting at a 0.8°C/s (#a) and solidification at 1°C/s (#b) and 4°C/s (#c). The numbers correspond to the various metallurgical reactions as presented in Tables 2a, b

Table 2a.

Non-equilibrium thermal characteristics of the AM50 alloy test samples obtained during the melting process at a 0.8°C/s heating rate

Points	Thermal characteristics	Melting rate, 0.8°C/s	
		Temp. °C ± STDEV	Fraction liquid, %
#1	Start of the alloy melting process (Solidus temperature)	433.7±1	0
#2	End of the $\alpha(\text{Mg})$ - $\beta(\text{Mg}_{17}\text{Al}_{12})$ eutectic phase melting	454.2±2.4	2.0
#3	End of the alloy melting process (Liquidus temperature)	640.1±1.5	100

most likely, nucleated from the melt. Latent heat evolved and caused the temperature of the surrounding melt to rise. This point was clearly visible as a sudden change in the first derivative curve (point #4 in Figure 3). With further cooling, the magnesium dendrites continued to grow. At 429.4°C the next change in the first derivative curve was observed and corresponded to the nucleation of the $\alpha(\text{Mg})$ - $\beta(\text{Mg}_{17}\text{Al}_{12})$ eutectic (point #5 in Figure 3). The cooling curve indicated that the latent heat of the $\alpha(\text{Mg})$ was sufficient to increase the temperature of the test specimen during the solidification process. This was manifested by the positive value of the first derivative curve (Figure 3). This phenomenon was related to the so-called recalescence effect [4-6, 19]. It was found that non-equilibrium solidus temperature was approximately 422.5°C. Presented thermal characteristics are in good agreement with these reported in the literature [2, 11, 22]. Comprehensive studies including thermal analysis experiments and thermodynamic calculations indicated the differences between the measured and calculated liquidus and solidus temperatures for the AM and AZ series alloys [20, 21].

The authors explanation pointed to the minute precipitation of the AlMn based phases not detected by the classical thermal analysis techniques. The practical impact of this phenomenon on the alloy structural and mechanical characteristics has to be determined especially for solidification conditions representative of industrial cast components under as-cast and heat treated conditions.

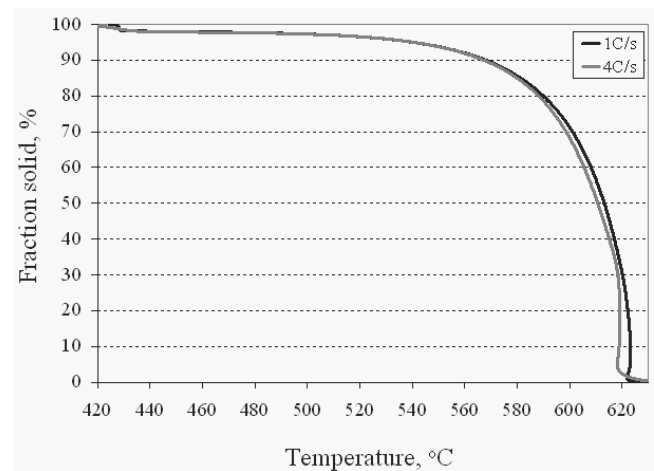


Fig. 4. Fraction solid vs. temperature curves of the AM50 alloy test samples that solidified at 1°C/s and 4°C/s average solidification rates

Table 2b.

Non-equilibrium thermal characteristics of the AM50 alloy test samples obtained during the solidification process at a 1 and 4°C/s solidification rates

Points	Thermal characteristics	Solidification rate, °C/s			
		1		4	
		Temp. °C ± STDEV	Fraction solid, %	Temp. °C ± STDEV	Fraction solid, %
#4	Nucleation of the $\alpha(\text{Mg})$ dendrites (Liquidus temperature)	625.1±0.9	0	636±0.5	0
#5	Beginning of nucleation of $\alpha(\text{Mg})$ - $\beta(\text{Mg} - \text{Mg}_{17}\text{Al}_{12})$ eutectic	429.4±1.9	98.2	439.7±1.1	97.9
#6	End of solidification (Solidus temperature)	422.5±1.1	100	397.1±2.6	100

The cooling curves for the AM50 alloy that solidified under a 4°C/s solidification rate are presented in Figures 2 and 3 (#c). It was observed that an instantaneous cooling rate reached up to 9°C/s within the liquid state. The shape of the first derivative curve remained similar as compared with cooling curve of the test sample that solidified under 1°C/s. It was observed that the beginning of the $\alpha(\text{Mg})$ dendrites' nucleation was shifted up by approximately 10°C, i.e., to 636°C as compared with the test sample that solidified under 1°C/s. Similar observations were made for the nucleation temperatures of the $\alpha(\text{Mg})$ - $\beta(\text{Mg}_{17}\text{Al}_{12})$ eutectic that was shifted up by approximately 10°C, i.e., to 439.7°C as compared with the test sample that solidified under a 1°C/s solidification rate. The dashed vertical lines in Figure 3 represent the maximum metallurgical reactions for the test sample that solidified under a 1°C/s cooling rate. It is worth noting that the maximum peak stayed within a $\pm 2^\circ\text{C}$ range for all analyzed conditions. Most likely the reason for the temperature shift of the nucleation temperatures is twofold. Firstly, this could be attributed to signal smearing caused by the temperature gradient within the test sample and the moving crystallization front. Secondly, this shift could be caused by localized variation of the liquid alloy composition resulting from the non-equilibrium solidification conditions. This could be a localized phenomenon characteristic of an undercooled melt where the diffusion process was restricted. The detailed contributions and the overall effect have to be validated and determined since this alloy is predominantly used for permanent mold applications where the solidification rates are very high and far from the equilibrium conditions. The smearing effect can be minimized by reducing the test sample mass and/or by optimizing the wall thickness to minimize the temperature gradient for the hollow test sample design.

Analysis of the fraction solid curves calculated for the 1 and 4°C/s solidification rates indicated that the volume of the solid phase rose to approximately 70% when the temperature dropped 20°C below the liquidus. The remaining 30% of the liquid solidified within $\alpha(\text{Mg})$ interdendritic spaces (Figure 4). This could have an impact on the feeding characteristics of the AM50 alloy. The increased solidification rate did not have a significant effect on the fraction solid evolution during the solidification process. This noticeable change was observed within the initial stage of the solidification process and the fraction solid curves reflected the shift in the non-equilibrium liquidus temperature most likely caused by an increased solidification rate.

3.2. Metallographic analysis

Metallographic observations of the AM50 test sample solidified at 1°C/s revealed the dendritic microstructure of the $\alpha(\text{Mg})$ matrix with visible eutectic regions distributed within the interdendritic spaces (Figures 5a-b). This observation was in agreement with the thermal analysis experiments where two distinct metallurgical reactions were noted on the cooling curve, i.e., nucleation of the $\alpha(\text{Mg})$ dendrites and the $\alpha(\text{Mg})$ - $\beta(\text{Mg}_{17}\text{Al}_{12})$ eutectic at approximately 625 and 429°C respectively (Table 2b). Image analysis showed that the average SDAS was $64.3 \pm 12.3 \mu\text{m}$ (Figure 6). Standard deviation represented approximately 20% of the overall SDAS value that was typical for a slowly solidified test sample with a heterogeneous microstructure. Metallographic observations of the AM50 test sample that solidified at a 4°C/s cooling rate revealed significant microstructural refinement caused by the thermal modification mechanism (Figures 5c-d). The SDAS was reduced to $43.4 \pm 9.7 \mu\text{m}$ as compared with $64.3 \pm 12.3 \mu\text{m}$ for the test sample that solidified at a 1°C/s cooling rate. The SDAS strongly depends on the increased solidification rate that reduced the time necessary for coarsening of the Mg dendrites and that resulted in multiplication of the secondary dendrite arms that distribute the solute content in front of the solidifying interface.

3.3. Melt cover gas and ignition test

Argon as a cover gas for laboratory melting/solidification experiments was utilized instead of the conventionally used CO_2/SF_6 that is recognized for its negative environmental impact. It is known that a significant contribution to the green house gas effect by the magnesium industry is due to SF_6 emissions. In general, inert gases alone such as Argon or Nitrogen provide some melt protection due to the partial formation of a protective layer on the liquid metal surface. The magnesium vapour can escape and form magnesium oxide often visible in the form of a white powder on the melt surface [23, 24]. Proper cover gas flow is required together with test chamber ventilation to prevent accumulation of unreactive magnesium vapor [24]. The robust apparatus [18] design, utilized in this study, minimized problems

associated with evaporation and reactivity of the processed magnesium alloys but at the same time did not compromise resolution of the thermal analysis signal.

The controlled ignition test showed that heating of the AM50 alloy test sample without a protective atmosphere resulted in a gradual oxidation process manifested as a carbon based, dark layer visible on the test sample surface (Figure 7a). Exceeding the solidus temperature ($\sim 434^{\circ}\text{C}$) during the melting cycle did not cause immediate alloy ignition but resulted in development of a white sponge-like Mg oxide layer on the top sample surface (Figure 7b). Oxide build up continued with the increasing temperature and led to test sample ignition at approximately 585°C (Figure 7c). Prior to ignition the localized burning was visible most likely caused by molten magnesium that penetrated the porous oxide layer and reacted with surrounding air [25]. Proper safety procedures for laboratory simulations of melting and solidification experiments requires an uninterrupted flow of Argon gas and a melting temperature up to 700°C . Consequently this could minimize the magnesium oxide build up associated with Argon use. It was found that utilizing Argon for gas quenching does not compromise its ability to protect the melt. Controlled ignition test can be used for evaluation of the effect of alloying additions such as Be, Ca on magnesium alloy's reactivity at elevated temperatures that can provide methodology for laboratory development of ignition-proof magnesium alloys. In turn, the utilization of the conventionally used cover gases like CO_2/SF_6 can be properly optimized. Consequently, this can minimize its negative environment impact [24]. Moreover, such experiments can be used for heat treatment optimization studies carried out to minimize oxidation process of magnesium alloys designated for high temperature applications.

3.4. Application of experimental results

The presented simulation methodology allows for the production of metallographic test samples for image analysis and related thermal characteristics for statistical analysis of their relationship. Comparative image analysis of the cast component and UMSA generated structures allows for the determination of the solidification characteristics of the component's given section. This information could be used for subsequent optimization of the metal casting processing technologies such as heat treatment. One of the examples could be a simulation of the semi-continuous heat treatment process like the T5 where the cast component is water quenched after the de-molding operation and subjected to the continuous artificial aging operation.

Moreover, this data provides valuable input for computer models like the fraction solid, non-equilibrium liquidus, solidus temperatures, etc. obtained for variable solidification rates. Additionally, the effect of thermal or chemical modification (grain refiners, eutectic modifiers, etc.) on selected thermal characteristics like undercooling temperature can be determined for specific solidification rates representative of specific casting processes (sand, permanent, etc.). Current computer simulation software relies on the thermal characteristics obtained during the equilibrium solidification conditions and does not address the effect of the thermal and chemical aspects of microstructure refinement.

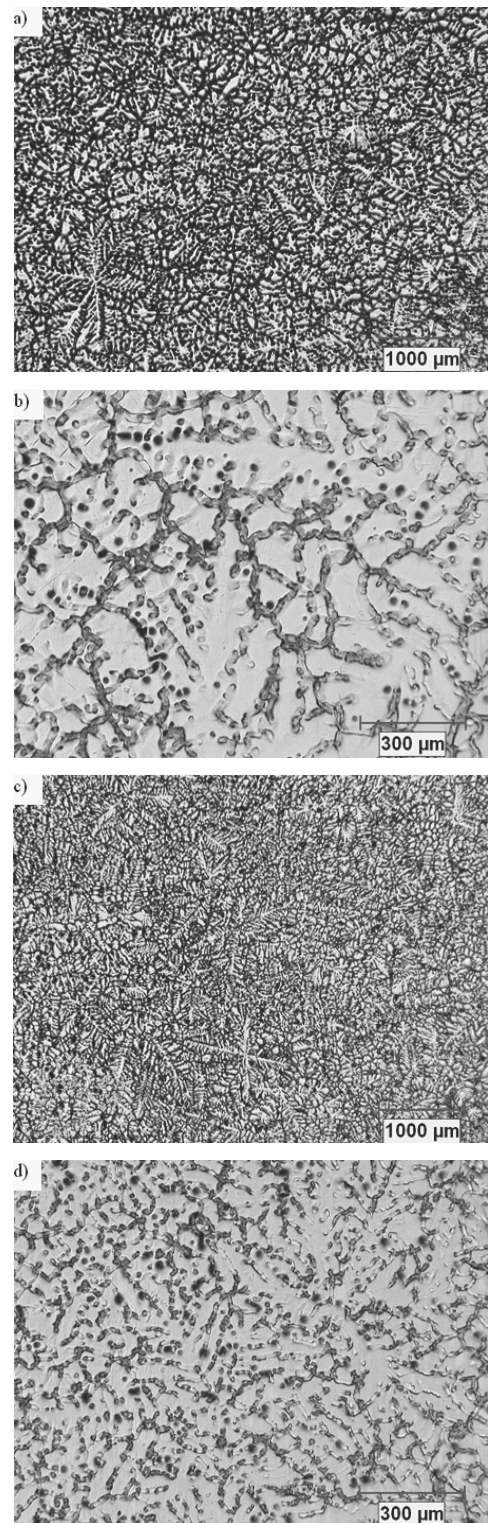


Fig. 5. Optical micrographs of the AM50 alloy test samples with corresponding SDAS under 50x (a-c) and 500x (b-d) magnifications that solidified at the following solidification rates: a-b) 1°C/s (SDAS = $64.3 \pm 12.3 \mu\text{m}$); c-d) 4°C/s (SDAS = $43.4 \pm 9.7 \mu\text{m}$)

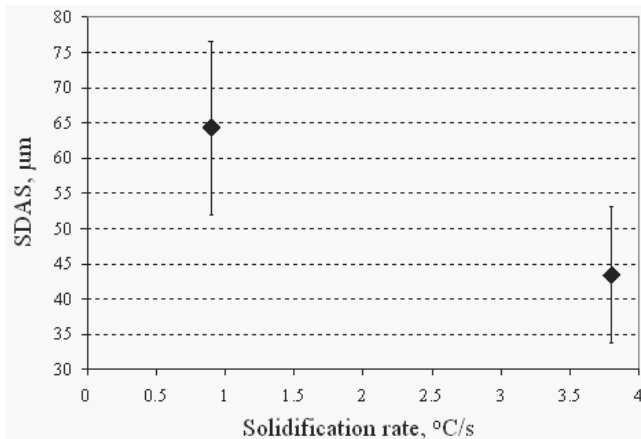


Fig. 6. Secondary Dendrite Arm Spacing (SDAS) with corresponding standard deviation of the AM50 alloy test samples that solidified at approximately 1 and 4°C/s solidification rates

4. Conclusions

Based on the solidification experiments and subsequent metallurgical analysis for the AM50 alloy the following conclusions could be made:

- It is feasible for a magnesium macro test sample to achieve a variable solidification rate, the corresponding microstructural refinement and to maintain good resolution of the thermal analysis signal.
- Generated microstructures at different cooling rate are representative of specific sections of the cast component and could be used for subsequent optimization of the casting post processing technologies like the heat treatment.
- Thermal analysis performed during solidification experiments at a 1 and 4°C/s average cooling rate had satisfactory signal resolution. This allowed for determination of the thermal characteristics and for correlation with alloy microstructural parameters.
- The start of the metallurgical reactions was shifted toward the higher values with increased solidification rates from 1 to 4°C/s, while first derivative peaks stayed within a $\pm 2^\circ\text{C}$ range.
- Increasing the solidification rate from 1 to 4°C/s decreased the SDAS of the magnesium matrix from 64.3 ± 12.3 to $43.4 \pm 9.7 \mu\text{m}$.
- Fraction liquid curve (obtained during the melting cycle) can provide valuable input for determination of the semi-solid processing parameters while fraction solid curves (obtained during the solidification cycle) can determine feeding characteristics of the AM50 alloy.
- Compressed Argon gas with variable flow rates could be used as a quenching medium for magnesium rapid solidification experiments as well as a cover gas to prevent test sample ignition during laboratory simulations.
- A controlled alloy ignition test indicated that exceeding the alloy melting temperature resulted in gradual surface oxidation followed by alloy ignition above 585°C.

- Thermal and structural characteristic data could provide valuable input for computer modeling software particularly for non-equilibrium solidification conditions.

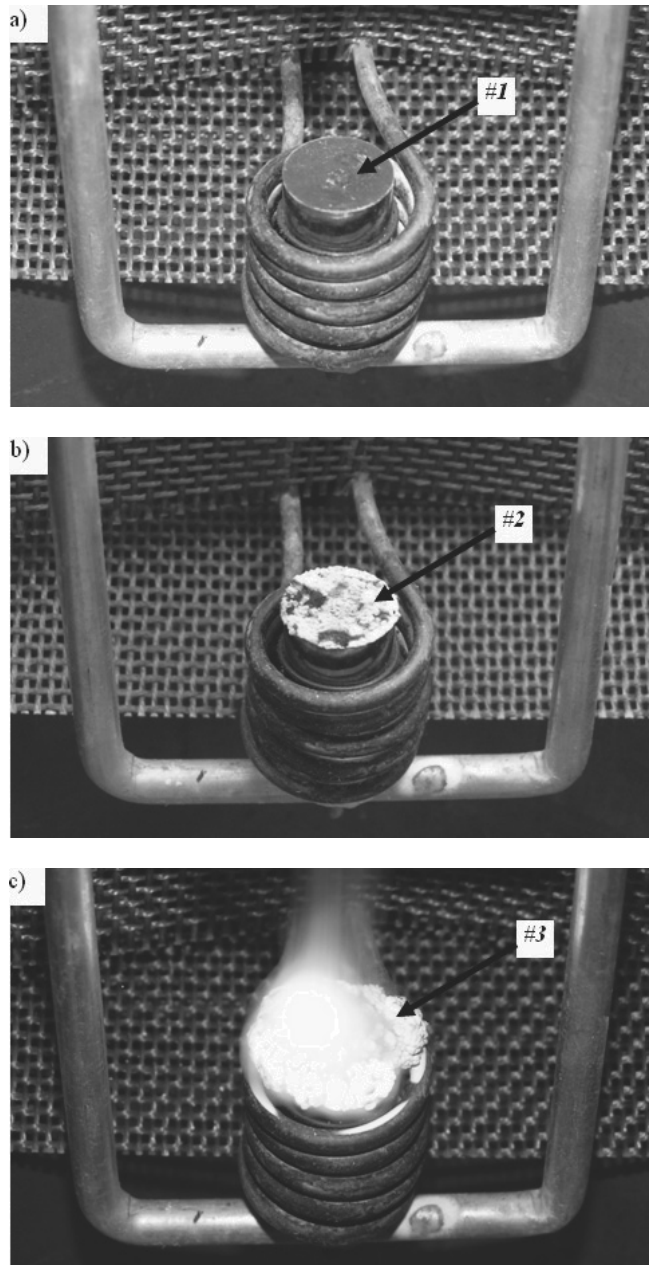


Fig. 7. Images of the AM50 alloy test sample during the melting process without cover gas. The test samples were heated to 700°C at a 0.8°C/s heating rate. The visual observations of the test sample surface were as follows: a) Development of dark, carbon based layer at approximately 540°C (#1); b) Development and growth of sponge-like white magnesium oxide at approximately 570°C (#2); c) Spontaneous test sample ignition at 585°C (#3)

Acknowledgements

The authors would like to thank Dr. M. Kasprzak from the Silesian University of Technology in Poland for his valuable contributions to the UMSA Technology Platform's configuration and R. Zavadil from CANMET-MTL for metallographic work. This research is co-funded by AUTO21, a member of the Network of Centres of Excellence of Canada program and within the framework of scientific financial resources of the Ministry of Science and High Education in Poland as a research and development project R15 0702 headed by Prof. L.A. Dobrzański.

References

- [1] B.L. Mordike, T. Ebert, Magnesium properties-applications-potentials, *Materials Science and Engineering A302* (2001) 37-45.
- [2] Y.W. Riddle, M.M. Makhlof, Characterizing solidification by non-equilibrium thermal analysis, *Proceedings of the 132nd TMS Annual Meeting "Magnesium Technology"*, San Diego, 2003, 101-106.
- [3] N. Saunders, X. Li, A.P. Miodownik, J-Ph. Schille, Modeling of the thermo-physical properties relevant to solidification, *Proceedings of the 10th International Conference "Modeling of Casting, Welding and Advanced Solidification Processes"*, 2003, 669-676.
- [4] H. Yamagata, H. Kurita, M. Aniolek, W. Kasprzak, J.H. Sokolowski, Thermal and metallographic characteristics of the Al-20%Si high-pressure die-casting alloy for monolithic cylinder blocks, *Journal of Materials Processing Technology* 199 (2007) 84-90.
- [5] L.A. Dobrzański, W. Kasprzak, J.H. Sokolowski, Analysis of the Al-Si alloy structure development using thermal analysis and rapid quenching techniques, *Proceedings of the 12th Scientific International Conference "Achievements in Mechanical and Materials Engineering" AMME'2003, Gliwice-Zakopane*, 2003, 225-228.
- [6] J. Chen, W. Kasprzak, J.H. Sokolowski, Metallurgical aspects of novel approach to reduce the heat treatment process for Al based alloys by utilization of heat from the solidification process, *Journal of Materials Processing Technology* 176 (2006) 24-31.
- [7] L. Han, H. Hu, D. Northwood, A comparative study on the solution treatment of Mg-Al and Mg-Al-Ca alloys, *Proceedings of the 137th TMS Annual Meeting "Magnesium Technology"*, New Orleans, 2008.
- [8] L. Han, H. Hu, D. Northwood, N. Lie, A calorimetric analysis of dissolution of second phases in as-cast AM50 alloys, *Proceedings of the 136th TMS Annual Meeting "Magnesium Technology"*, Orlando, 2007, 369-373.
- [9] Y. Fasoyinu, J. Barry, M. Sahoo, P. Labelle, D. Wang, R.A. Overfelt, Thermophysical properties of magnesium alloys AE42, AJ52X and AM60B, *AFS Transactions* 111 (2003) 1031-1052.
- [10] H. Onda, K. Sakurai, T. Masuta, K. Oikawa, K. Anzai, W. Kasprzak, J.H. Sokolowski, The effect of solidification models on the prediction results of the temperature change of the aluminum cylinder head estimated by FDM solidification analysis, *Materials Science Forum* 561-565 (2007) 1967-1970.
- [11] M.M. Avedesian, H. Baker, *Magnesium and Magnesium Alloys*, ASM International, Ohio, 1999.
- [12] Y. Fasoyinu, P. Newcombe, M. Sahoo, Lost foam casting of magnesium alloys AZ91D and AM50, *AFS Transactions* 114 (2006) 707-718.
- [13] V.Y. Gertsman, J. Li, S. Xu, J.P. Thomson, M. Sahoo, Microstructure and second phase particles in low and high pressure die cast magnesium alloy AM50, *Metallurgical and Materials Transactions* 36A/8 (2005) 1989-1997.
- [14] F. Habashi, *Alloys-Preparation, Properties, Applications*, Wiley-VCH, Weinheim, 1998.
- [15] A. Luo, H. Hu, J. Lo, Microstructure and mechanical properties of squeeze cast AZ91D magnesium alloy, *Light Metals* (1996) 377-387.
- [16] A. Luo, Magnesium: current and potential automotive applications, *JOM* 54/2 (2002) 42-48.
- [17] A. Luo, A.K. Sachdev, P.H. Fu, L.M. Peng, H.Y. Jiang, C.Q. Zhai, Y.D. Yu, Low pressure die casting of AZ91 and AM50 magnesium alloys, *AFS Transactions* (2008).
- [18] J.H. Sokolowski, W.T. Kierkus, M. Kasprzak, W. Kasprzak, US Patent No. 7,354,491 B2 (2008).
- [19] W.T. Kierkus, J.H. Sokolowski, Recent advances in CCA: A new method of determining baseline equation, *AFS Transactions* 14 (1999) 161-167.
- [20] D. Mirkovic, R. Schmid-Fetzer, Solidification curves for commercial Mg alloys determined from differential scanning calorimetry with improved heat-transfer modeling, *Metallurgical and Materials Transactions* 38A (2007) 2575-2592.
- [21] M. Ohno, D. Mirkovic, R. Schmid-Fetzer, Phase equilibria and solidification of Mg-rich Mg-Al-Zn alloys, *Materials Science and Engineering A* 421 (2006) 328-337.
- [22] Y.W. Riddle, L.P. Barber, M.M. Makhlof, Characterization of Mg solidification and as-cast microstructures, *Magnesium Technology* (2004) 203-208.
- [23] J.W. Fruehling, J.D. Hanawalt, Protective atmospheres for melting magnesium alloys, *Modern Casting* 56/2 (1969) 159-164.
- [24] Ch. Tian, D. Albright, *Fundamentals of magnesium melt handling in the die casting foundries*, *Die Cast Engineer* (2003) 38-44.
- [25] T-S. Shih, J-H. Wang, K-Z. Chong, Combustion of magnesium alloys in air, *Materials Chemistry and Physics* 85 (2004) 302-309.
- [26] L.A. Dobrzański, T. Tański, L. Čížek, Z. Brytan, Structure and properties of the magnesium casting alloys, *Journal of Materials Processing Technology* 192-193 (2007) 567-574.
- [27] L.A. Dobrzański, T. Tański, L. Čížek, Characterization of MCMgAl9Zn1 MCMgAl6Zn1 magnesium alloys structure, *Journal of Materials Engineering* 157-158 (2007) 381-386.
- [28] L.A. Dobrzański, T. Tański, L. Čížek, Heat treatment impact on the structure of die-cast magnesium alloys, *Journal of Achievements in Materials and Manufacturing Engineering* 20 (2007) 431-434.
- [29] L.A. Dobrzański, T. Tański, J. Trzaska, L. Čížek, Modelling of hardness prediction of magnesium alloys using artificial neural networks applications, *Journal of Achievements in Materials and Manufacturing Engineering*, 26/2 (2008) 187-190.